RSC Advances

ROYAL SOCIETY OF CHEMISTRY

www.rsc.org/advances

Journal Name

RSC Publishing

ARTICLE

Facile synthesis of (Ni,Co)@(Ni,Co)$_x$Fe$_{3-x}$O$_4$ core@shell chain structures and (Ni,Co)@(Ni,Co)$_x$Fe$_{3-x}$O$_4$/graphene composites with enhanced microwave absorption†

Cite this: DOI: 10.1039/x0xx00000x

Received 00th February 2015,
Accepted 00th February 2015

DOI: 10.1039/x0xx00000x

www.rsc.org/

Yuan Lin, Lu Xu, Zhiyuan Jiang,* Hongli Li, Zhaoxiong Xie and Lansun Zheng

Abstract: A facile strategy was developed to synthesize a series of multiple metal@metal oxide hybrid structures, such as (Ni,Co)@(Ni,Co)$_x$Fe$_{3-x}$O$_4$, Ni@Ni$_x$Fe$_{3-x}$O$_4$, Co@Co$_x$Fe$_{3-x}$O$_4$, and (Ni,Co)@Ni$_x$Co$_{3-x}$O$_4$. The (Ni,Co)@(Ni,Co)$_x$Fe$_{3-x}$O$_4$ core@shell chain structures display enhanced microwave absorption performance compared with other hybrid structures. The (Ni,Co)@(Ni,Co)$_x$Fe$_{3-x}$O$_4$ demonstrates not only a combination of the distinct component properties but also a synergy between different components. By introducing graphene into a composite system—(Ni,Co)@(Ni,Co)$_x$Fe$_{3-x}$O$_4$/graphene, much better microwave absorption performance can be achieved. Its reflection loss value can reach -30.34 dB at 8.48 GHz with a thickness of 2.5 mm and its absorption bandwidth with the reflection loss below -10 dB is about 7 GHz from 9.12 to 16.08 GHz with a thickness of 2.0 mm. Our study illustrates the feasibility that microwave absorption materials with strong absorption property as well as lightweight and broad absorption frequency range can be rationally designed by constructing hybrid structures and composites.

Introduction

Microwave absorption materials have attracted great interest in the past decade because of the continuous growth in the demands for the reduction of electromagnetic radiation and the improvement of anti-electromagnetic interference.[1-4] A ideal microwave absorption material should bear some basic properties, such as strong absorption, broad absorption frequency range, low density, and thin-coating capability for production. Due to their high magnetization, magnetic metals and metal oxides were studied extensively as microwave absorption materials with high absorption strength.[5-10] However, a single layer of any of these materials can only absorb the electromagnetic wave in a specific frequency range. For example, the bandwidth corresponding to reflection loss (RL) below -10 dB of a single layer of W-type Ba(Zn$_{0.5}$Co$_{0.5}$)$_2$Fe$_{16}$O$_{27}$, a typical ferrite, is about 3.0 GHz (8.7 GHz-11.7 GHz) with a thickness of 2 mm.[5] The effective absorption (RL<-10 dB) frequency range of Fe nanowires prepared by chemical vapour deposition is about 5 GHz (7-12 GHz) with a thickness of 2.0 mm.[11] Though multilayer configuration can effectively enlarge the absorption frequency range, it increases the thickness of the coating layer and requires very complicated construction technology. Furthermore, it is difficult for single material to achieve impedance match conditions, which is important for microwave absorption materials. Therefore, constructing hybrid nanostructures, such as core@shell nanostructures,[12, 13] heterostructured nanocrystals,[14, 15] and nanocomposites[16, 17] has become a new strategy to design and fabricate microwave absorption materials.

Another class of important microwave absorption materials studied is carbon materials, such as graphene and carbon nanotubes, due to their low density, great flexibility as well as unique electrical/mechanical properties.[18, 19] The composites of magnetic materials and graphene usually have wider effective absorption frequency range because of the interfacial electronic interaction between magnetic particle and graphene.[20-22] For instances, graphene coated Fe nanocomposites exhibit a wide frequency range about 4.4 GHz when RL <−10 dB with the thickness of 2.0 mm.[20] The absorption bandwidth for the graphene/Fe$_3$O$_4$@Fe/ZnO quaternary nanocomposites can reach up to 4 GHz (from 14 to 18 GHz) with the thickness of 2.0 mm. [21] However, the search of microwave absorption materials with much broader absorption frequency range as well as stronger absorption properties still remains as a great challenge.

Herein, based on the activity order of metals, a facile strategy combined with solvothermal synthesis and partial oxidation process was developed to synthesize series of metal@metal oxides structures, such as (Ni,Co)@(Ni,Co)$_x$Fe$_{3-x}$O$_4$, Ni@Ni$_x$Fe$_{3-x}$O$_4$, Co@Co$_x$Fe$_{3-x}$O$_4$ and (Ni,Co)@Ni$_x$Co$_{3-x}$O$_4$. Among these hybrid structures, (Ni,Co)@(Ni,Co)$_x$Fe$_{3-x}$O$_4$ chain structures show the best microwave absorption performance. By incorporating graphene to assemble a composite material—(Ni,Co)@(Ni,Co)$_x$Fe$_{3-x}$O$_4$/graphene, the effective absorption (RL<-10 dB) frequency range can be achieved about 7 GHz from 9.12 to 16.08 GHz with a thickness of 2.0 mm, which is significantly wider than other similar reported results.

Materials and methods

Materials

Cobalt (II) acetylacetionate ($Co(acac)_2$, 98.0%), Nickel (II) acetylacetionate ($Ni(acac)_2$, 98.0%), Ferric (III) acetylacetionate ($Fe(acac)_3$, 98.0%) were purchased from Alfa Aesar, a Johnson Matthey Company. Oleylamine (OAm, 80-90%), Oleic acid (OA, 90%), 1-octadecene (ODE, 90%) were obtained from Beijing InnoChem Science & Technology Co., Ltd. N, N-Dimethylformamide (DMF), and ethanol of analytical reagent grade were obtained from Sinopharm Chemical Reagent Company. Graphene was purchased from XFNANO Technology Co., LTD.

Synthesis of (Ni,Co)@(Ni,Co)$_x$Fe$_{3-x}$O$_4$ chain structures

Transition-metal compounds, $Co(acac)_2$ (300 mg, 0.0012 mol), $Ni(acac)_2$ (300 mg, 0.0012 mol) and $Fe(acac)_3$ (300 mg, 0.0008 mol) were dissolved in 48.5 mL DMF, then a mixture of 12 mL Oleylamine, 8 mL 1-octadecene and 1.5 mL Oleic acid was added to the solution. The mixed solution was transferred to a 100 mL Teflon-lined stainless-steel autoclave which was heated at 180 °C for 24 h before cooled to room temperature. The black precipitate was collected by centrifugation and washed with ethanol three times. The final products were obtained by heating the washed precipitate at 350 ^{o}C for 2 h in ambient atmosphere.

Preparation of (Ni,Co)@(Ni,Co)$_x$Fe$_{3-x}$O$_4$/graphene composites

(Ni,Co)@(Ni,Co)$_x$Fe$_{3-x}$O$_4$ (97 mg) and graphene (3 mg) were dispersed in ethanol and sonicated for 0.5 h. The black precipitates were isolated by centrifugation, washed with absolute ethanol and dried at 70 °C for 8h.

Characterization

X-ray diffraction (XRD) data was collected on Rigaku Ultima IV with Cu Kα radiation. The morphology of the products was investigated using scanning electron microscopy (SEM, Zeiss Sigma, 20kV) and transmission electron microscopy (TEM, Philips, Tecnai, F20, 200kV, F30, 300kV). Elemental mapping images were performed with an Energy Dispersive X-ray Detector (EDX) system attached to TEM. For TEM-EDX analysis, the samples were dispersed on carbon coated two-layer copper grid. X-ray photoelectron spectroscopy (XPS) analysis was performed on PHI Quantum 2000. The magnetic characterizations of samples were measured by a vibrating sample magnetometer (VSM, Lake Shore).

Electromagnetic measurements

Samples used in electromagnetic measurements were prepared by thoroughly mixing active materials ((Co,Ni)@(Ni,Co)$_x$Fe$_{3-x}$O$_4$ (50 mg), or (Co,Ni)@(Ni,Co)$_x$Fe$_{3-x}$O$_4$/graphene (50 mg)) with paraffin matrix (50 mg). These samples were then compressed into a toroidal shape (Φ_{out} = 7.00 mm and Φ_{in} = 3.00 mm) with the spreading thickness of about 2 mm. The effective complex permittivity and permeability were measured using an Agilent vector network analyzer (85071E) from 2-18 GHz via Nicolson-Ross method.[23]

Results and discussion

Structure and morphologies analysis

Figure 1a shows the SEM image of the (Ni,Co)@(Ni,Co)$_x$Fe$_{3-x}$O$_4$. It is corral-like structure with long chains made of irregular beads with the diameter of about 1 μm. The XRD pattern of the sample is shown in Figure 1b, the diffraction peaks can be divided into two sets. The first set of peaks (29.9°, 35.3°, 43.4°, 57.3°, and 62.9°) can be indexed as a cubic structure (Fd-3m) with a = 8.3427. This cell parameter is very similar to those of $NiFe_2O_4$ (PDF No. 00-010-0325), $CoFe_2O_4$ (PDF No. 00-022-1086) and Fe_3O_4 (PDF No. 03-065-3107). The second set of peaks (44.4°, 51.6°, and 76.1°) can be indexed as cubic Ni (PDF No. 03-065-2865) or Co (PDF No. 00-001-1255). The compositional information was provided by EDX analysis (Figure 1c, 1d). Four elements, Co, Ni, Fe and O can be easily detected. Ni is mainly located in the centre, Fe is mainly located on the outer shell layer, and Co is concentrated between the Ni core and the Fe shell. The distribution of O is almost coincided with that of Fe element and is distributed in the outer layer of the chain structures, suggesting that the outer layer of the sample is metal oxide. The core@shell structures can be confirmed by cross-sectional composition line profiles (Figure 1e). The concentrations of Fe and Co have two peaks located on the shell area while the concentration of Ni only has a peak centred on the core area. These results are consistent with the core@shell structure. By observing carefully, it could be found that the profile of Ni extends to the shell area, indicating the existence of small amount of Ni in the shell layer. Further evidences of the structural composition come from the XPS investigation (Figure S1†), which reveals that the elements Fe, Co and Ni are existed as Fe_3O_4, CoO and NiO on the surface. Figure 1f shows the HRTEM image recorded from a junction area of the core@shell structure. The shell layer can be easily identified due to their weak contrast. The lattice spacing of 0.25 nm observed in the shell area is quite consistent with those of (311) planes of $NiFe_2O_4$, $CoFe_2O_4$, and Fe_3O_4. These results suggest that the composition of the outer layer is (Ni,Co)$_x$Fe$_{3-x}$O$_4$. Although Ni core and Co metal were detected by XRD, the XPS peaks of Ni^0 and Co^0 were not observed, which is attributed to the limited penetration depth of XPS itself.

Based on these experiment results, it is reasonable to conclude that the as-prepared long chain structures have a core@shell structure. The core mainly consisted of Ni, Co metal and the shell was mainly iron oxides containing small amount of NiO and CoO. Furthermore, by choosing suitable metal acetylacetionate as precursors, other hybrid structures, such as Ni@Ni$_x$Fe$_{3-x}$O$_4$ (Figure S2†), Co@Co$_x$Fe$_{3-x}$O$_4$ (Figure S3†), and (Ni,Co)@Ni$_x$Co$_{3-x}$O$_4$ (Figure S4†) hybrid structures can also be prepared. It should be pointed out that the dense (Ni,Co)$_x$Fe$_{3-x}$O$_4$ layer could help retain the core@shell structures and the magnetic metal core (*e.g.* Ni) is necessary for the stable chain structures due to its stability and magnetic performance.

Due to their similar atomic radius, Ni, Co and Fe atoms can diffuse into the crystal structure of each other and form alloy structures, thus the inhomogeneous redistribution of these elements must resulted from oxidation process. Considering the differences between the standard reduction potentials (SRP) of the Ni^{2+}/Ni pair (-0.25 V vs. NHE), Co^{2+}/Co pair (-0.28 V vs. NHE) and Fe^{3+}/Fe^{2+} pair (+0.77 V vs. NHE), Fe^{2+}/Fe pair (-0.44 V vs. NHE), Ni^{2+} is the most easily to be reduced and Fe^{2+} is the most difficult to be reduced. During the oxidation process, iron in the outer layer is the easiest to be oxidized

to iron oxides, thus iron is accumulated in the outer layer with some cobalt and nickel. As the dense $(Ni,Co)_xFe_{3-x}O_4$ layer forms, further oxidation of the inner layer is prevented, therefore Ni, which is the most difficult to be oxidized among these metals will accumulate in the core.

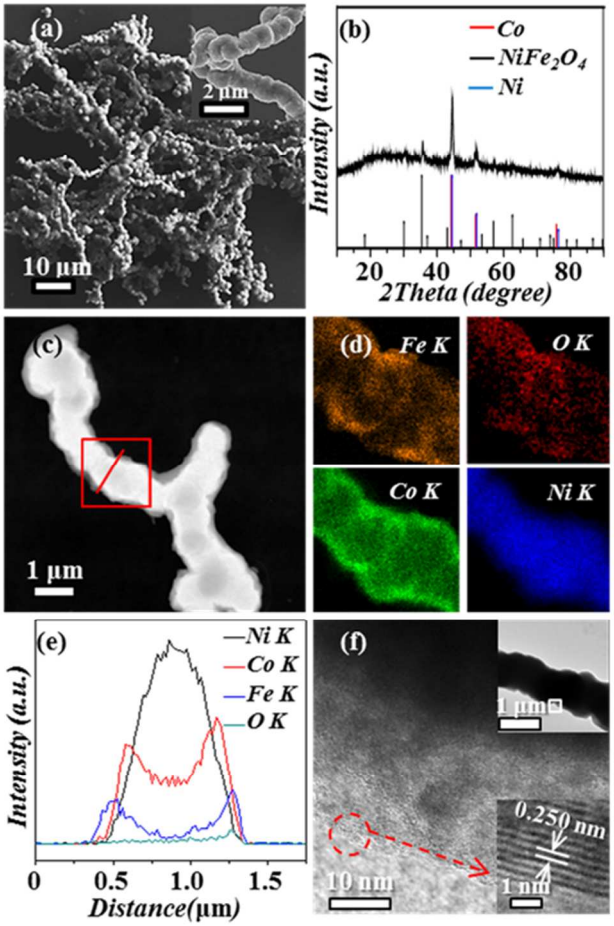

Figure 1 (a) Typical SEM image, (b) XRD pattern, (c) the HAADF image, (d) elemental maps, (e) the cross-sectional compositional line profiles and (f) HRTEM images of $(Ni,Co)@(Ni,Co)_xFe_{3-x}O_4$ core@shell chain structures. Inset in a) is enlarged SEM image, which shows the chain structure clearly; insets of f) are corresponding low magnification TEM image and enlarged HRTEM image.

The SEM image of $(Ni,Co)@(Ni,Co)_xFe_{3-x}O_4$/graphene composites was shown in Figure 2a. The chain structures of $(Ni,Co)@(Ni,Co)_xFe_{3-x}O_4$ are well kept and they are randomly distributed in the composites, whereas the smooth graphene is also observable. The presence of graphene can also be proved by the corresponding XRD pattern (Figure 2b) and Raman spectrum (Figure 2c). As shown in Figure 2b, the strong diffraction peak at 26.6° (2θ) is ascribed to the graphene sheets. Other peaks of the composites belong to $(Ni,Co)@(Ni,Co)_xFe_{3-x}O_4$ hybrid structures. Figure 2c shows the Raman spectrum of the composites, the intense feature around 1326, 1574, 2686 cm^{-1} is the characteristic bands of D, G and 2D bands. The D band originates form the breathing vibrations of aromatic rings in the honeycomb lattice. The G peak is due to the doubly degenerate zone center E_{2g} mode. The 2D is the second order of zone-boundary phonons. These results suggest that the graphene in the composites is few-layer stacked.

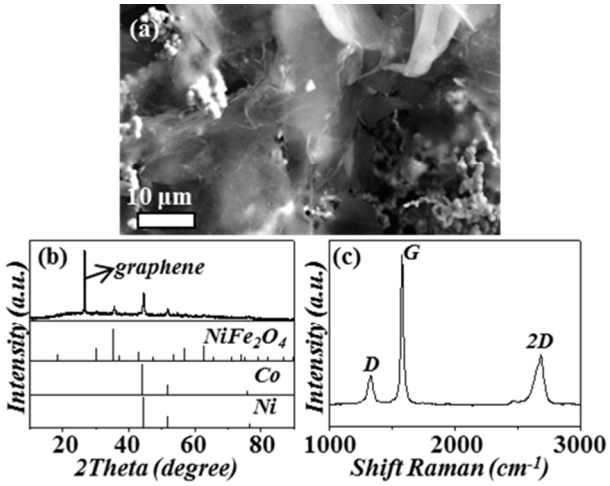

Figure 2 (a) SEM image, (b) XRD pattern and (c) Raman spectrum of $(Ni,Co)@(Ni,Co)_xFe_{3-x}O_4$/graphene composites.

Magnetic characterization

Fe, Co and Ni are all well-known ferromagnetic metals and many of their oxides are also reported ferrimagnetism at room temperature.[24, 25] Magnetic property of a material depends on its structure, shape anisotropy and crystallinity. The magnetic property of a material can greatly affect their microwave absorption performance, thus, the magnetic properties of $(Ni,Co)@(Ni,Co)_xFe_{3-x}O_4$ hybrid structures and $(Ni,Co)@(Ni,Co)_xFe_{3-x}O_4$/graphene composites were measured by a vibrating sample magnetometer (VSM) with fields up to 20 kOe at room temperature. The magnetic hysteresis loops (M-H loops) of the two samples were shown in Figure 3. The saturation magnetization (M_S) value of $(Ni,Co)@(Ni,Co)_xFe_{3-x}O_4$ is about 75.26 emu/g and the coercivity (H_C) value is 121.24 Oe. The M_S strongly depends on the chemical composition of the local environment of atoms and their electronic structure. The H_C is highly structural-sensitive and originates from the displacement of the domain wall. The M_S value for $(Ni,Co)@(Ni,Co)_xFe_{3-x}O_4$ is lower than those of the bulk materials because the spin disorder on the surface and surface oxidation would significantly reduce the total magnetic moment. The M_S and H_C values of $(Ni,Co)@(Ni,Co)_xFe_{3-x}O_4$/graphene are 58.56 emu/g and 119.26 Oe, respectively. In the present case, the decrease in magnetism of $(Ni,Co)@(Ni,Co)_xFe_{3-x}O_4$/graphene can be attributed mainly to the presence of nonmagnetic graphene in the composites. The $(Ni,Co)@(Ni,Co)_xFe_{3-x}O_4$ particles separated by graphene may further reduce their magnetic attraction.[26] The magnetization can also be visually shown by placing a magnet next to glass bottles filled with the ethanol dispersion of prepared $(Ni,Co)@(Ni,Co)_xFe_{3-x}O_4$ and $(Ni,Co)@(Ni,Co)_xFe_{3-x}O_4$/graphene composites. Both of the dispersed phases move quickly along the magnetic field and accumulate near the magnet within a few minutes (inset of Figure 3). These results prove that the as-prepared products are ferro-/ferri-magnetism.

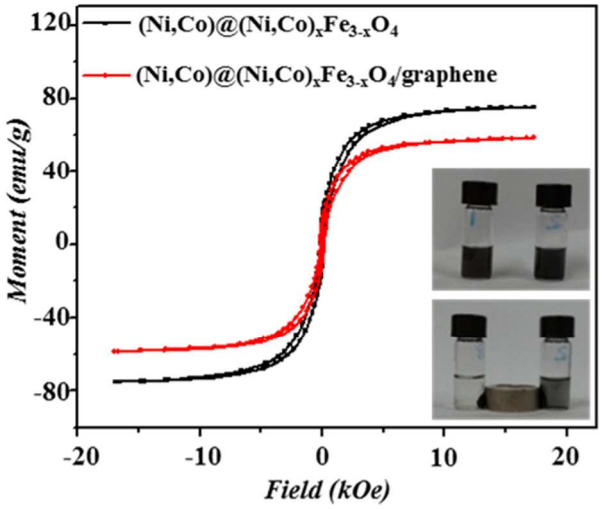

Figure 3 Room-temperature magnetization curve of as-prepared (Ni,Co)@(Ni,Co)$_x$Fe$_{3-x}$O$_4$ and (Ni,Co)@(Ni,Co)$_x$Fe$_{3-x}$O$_4$/graphene. (The inset photos show (Ni,Co)@(Ni,Co)$_x$Fe$_{3-x}$O$_4$ at the left side and (Ni,Co)@(Ni,Co)$_x$Fe$_{3-x}$O$_4$/graphene composites at the right side.)

Electromagnetic properties

To investigate the microwave absorption properties of these materials, the complex permittivity ($\varepsilon_r = \varepsilon' - j\varepsilon''$) and complex permeability ($\mu_r = \mu' - j\mu''$) of (Ni,Co)@(Ni,Co)$_x$Fe$_{3-x}$O$_4$ chain structures and (Ni,Co)@(Ni,Co)$_x$Fe$_{3-x}$O$_4$/graphene composites were measured by a vector network analyzer. Figure 4a shows the real part (ε') and imaginary part (ε'') of each sample. The real part (ε') is associated with the amount of polarization and imaginary part (ε'') is related to the dissipation of energy. For these two samples, the ε' values increased from 2 to 8 GHz followed with a rapid decrease between 8 and 11 GHz and a relatively slower increase between 11 and 18 GHz. For (Ni,Co)@(Ni,Co)$_x$Fe$_{3-x}$O$_4$ chain structures, there are two peaks of ε'' at 8.88 GHz and 14.72 GHz. The dielectric behaviour are due to intrinsic electric dipole, electronic spin and charge polarization on the response of (Ni,Co)@(Ni,Co)$_x$Fe$_{3-x}$O$_4$ core-shell sructure.[7, 27] The enhanced polarization in the mixed (Ni,Co)$_x$Fe$_{3-x}$O$_4$ crystals is attributed to the lattice distortion and an increase of trivalent ion concentration. According to the free-electron theory, $\varepsilon'' = 1/2\,\pi\varepsilon_0\rho f$, ($\rho$ is the resistivity), the ε'' peak is proportional to the resonance of dipolar polarization relaxation from the heterogeneous system. In this unique heterogeneous system, the effectiveness of isolation of the Co, Ni particles by the outer oxide layer may result in high resistivity.[11] For (Ni,Co)@(Ni,Co)$_x$Fe$_{3-x}$O$_4$/graphene composites, the maximum value of ε'' is 3.68 at 9.52 GHz and 2.47 at 15.68 GHz. The (Ni,Co)@(Ni,Co)$_x$Fe$_{3-x}$O$_4$/graphene composites is also a heterogeneous system with space charge polarization and the accumulation of virtual charges of two media, which is associated with the loss mechanism as Maxwell-Wagner polarization.[28]

Figure 4b presents the real part and imaginary part of permeability (μ' and μ'') of these two samples. The real part (μ') is the intrinsic magnetic property and the imaginary part (μ'') is the magnetic loss. The real part of permeability μ' stems from the cooperative effect of the domain wall resonance and spin rotational resonance of Ni. These two samples show a general decaying behaviour towards higher frequency for effective real and imaginary permeability value. The permeability value of (Ni,Co)@(Ni,Co)$_x$Fe$_{3-x}$O$_4$/graphene always remains higher than that of (Ni,Co)@(Ni,Co)$_x$Fe$_{3-x}$O$_4$, indicating a better magnetic loss that may result in a better microwave absorption performance. Magnetic loss could be attributed to eddy current loss with the formation of flaky structure and the size.[29-32]

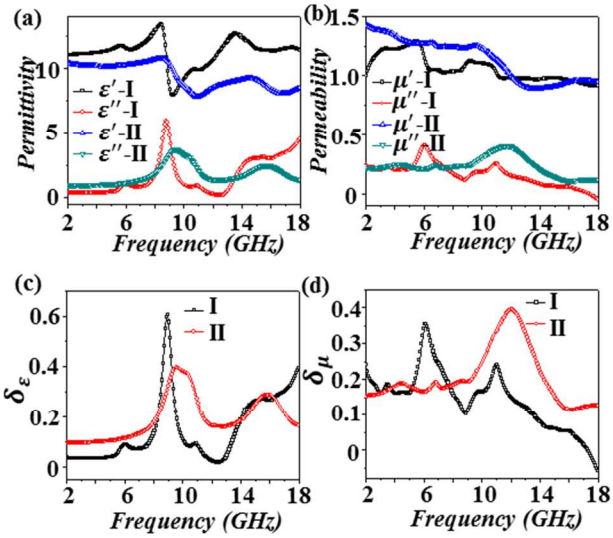

Figure 4 (a) The effective complex permittivity, (b) the effective complex permeability, (c) the dielectric loss tangent and (d) the magnetic loss tangent for (Ni,Co)@(Ni,Co)$_x$Fe$_{3-x}$O$_4$ chain structures (Sample I) and (Ni,Co)@(Ni,Co)$_x$Fe$_{3-x}$O$_4$/graphene composites (Sample II).

The dielectric loss and magnetic loss are the two major possible contributions for microwave absorption. The dielectric loss tangents ($\delta_\varepsilon = arc\tan\frac{\varepsilon''}{\varepsilon'}$) and magnetic loss tangent ($\delta_\mu = arc\tan\frac{\mu''}{\mu'}$) are calculated and shown in Figure 4c, 4d. The dielectric loss tangents and magnetic loss tangent are mainly originated from electronic polarization, ion polarization, intrinsic electric dipole polarization and their magnetic properties, which are dependent on their crystal structure, size and geometrical morphology. It can be found that both of the magnetic loss and dielectric loss play the vital role in the microwave absorption. In Figure 4c, the main δ_ε peak for (Ni,Co)@(Ni,Co)$_x$Fe$_{3-x}$O$_4$/graphene composites is broader than that of (Ni,Co)@(Ni,Co)$_x$Fe$_{3-x}$O$_4$, which may derive from the interfacial polarization relaxation between (Ni,Co)@(Ni,Co)$_x$Fe$_{3-x}$O$_4$ and graphene. In Figure 4d, the δ_μ value of (Ni,Co)@(Ni,Co)$_x$Fe$_{3-x}$O$_4$/graphene is higher than that of the (Ni,Co)@(Ni,Co)$_x$Fe$_{3-x}$O$_4$ from 8.0 GHz to 18.0 GHz. It can be ascribed to the high conductivity and polarization ability due to the variations of particle morphology and crystallinity.[32] It can also be found that both of the two samples hold good complementarities between the dielectric loss and the magnetic loss, suggesting that they may provide an improvement of microwave absorption activity.

Microwave absorption properties

To investigate the microwave absorption properties, the reflection loss (RL) of these samples were evaluated from the measured complex permittivity and permeability using the following equations:

$$\mathrm{RL\ (dB)} = -20\log\left|\frac{Z_{in}-1}{Z_{in}+1}\right| \quad (1)$$

While the normalized input impedance Z_{in} is calculated by the follows:

$$Z_{in} = \sqrt{\frac{\mu_r}{\varepsilon_r}}\tanh\left(j\frac{2\pi f d}{c}\sqrt{\mu_r\varepsilon_r}\right) \quad (2)$$

where *f* is the microwave frequency, *d* is the thickness of the absorber, and *c* is the velocity of electromagnetic wave in vacuum. ε_r, μ_r are relative effective complex permittivity and permeability, respectively.

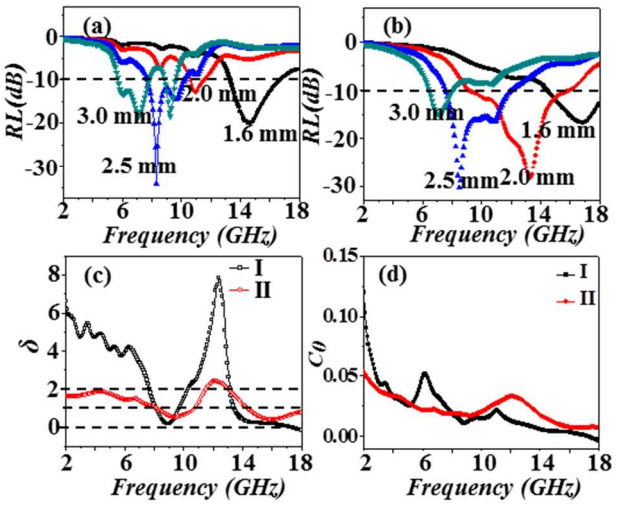

Figure 5 The calculated reflection loss for (a)(Ni,Co)@(Ni,Co)$_x$Fe$_{3-x}$O$_4$ chain structures (Sample I) and (b) (Ni,Co)@(Ni,Co)$_x$Fe$_{3-x}$O$_4$/graphene composites (Sample II) with different thicknesses in the frequency range of 2–18 GHz. (c) The calculated coefficient of electromagnetic matching (δ) and (d) C_0-f curves of the as-prepared samples.

As shown in Figure 5a, the sample (Ni,Co)@(Ni,Co)$_x$Fe$_{3-x}$O$_4$ (Sample I) exhibits excellent microwave absorption performance. With a sample thickness of only 1.6 mm, the RL value is under -10 dB from 13.36 to 16.72 GHz. When the thickness increased to 2.5 mm, the strongest RL (-34.1 dB) peak is obtained at 8.32 GHz and the effective absorption (RL<-10 dB) frequency ranges is about 2.4 GHz (from 7.76 - 10.16 GHz). To investigate the effect of composition to the absorption properties, the electromagnetic properties and microwave absorption properties of other hybrid structures were also evaluated. It can be found that Ni@Ni$_x$Fe$_{3-x}$O$_4$ (Figure S5†), Co@Co$_x$Fe$_{3-x}$O$_4$ (Figure S6†), and (Ni,Co)@Ni$_x$Co$_{3-x}$O$_4$ (Figure S7†) showed much weaker microwave absorption properties than (Ni,Co)@(Ni,Co)$_x$Fe$_{3-x}$O$_4$. While the absorption peaks of the three samples located in different frequencies and the contained cobalt oxides can effectively broaden the absorption bandwidth. These results indicated that the (Ni,Co)@(Ni,Co)$_x$Fe$_{3-x}$O$_4$ demonstrates not only a combination of the distinct component properties but also a synergy between different components. Its chain structures may induce magnetic interactions between the neighboring particles, which will improve the absorption performance.[33, 34] The interfacial polarization is induced by multiple interfaces in the (Ni,Co)@(Ni,Co)$_x$Fe$_{3-x}$O$_4$ core@shell structures, and the charge-carrier transfers between Ni, Co and (Ni,Co)$_x$Fe$_{3-x}$O$_4$ may also play a critical role to the improvement of the microwave absorption properties. [21, 35, 36]

Figure 5b shows the calculated reflection loss of (Ni,Co)@Ni,Co)$_x$Fe$_{3-x}$O$_4$/graphene based sample (sample II). The absorption bandwidths was largely broadened when the (Ni,Co)@(Ni,Co)$_x$Fe$_{3-x}$O$_4$ hybrid structures were coupled with graphene. A bandwidth corresponding to the RL below -10 dB is about 7.0 GHz (from 9.12 GHz to 16.08 GHz) with the sample thickness of 2 mm. When the thickness increases to 2.5 mm, the strongest RL is -30.34 dB at 8.48 GHz, which is comparable to that of (Ni,Co)@(Ni,Co)$_x$Fe$_{3-x}$O$_4$. Its effective absorption (RL<-10 dB) frequency range is still 4.32 GHz (from 7.68 GHz to 12.0 GHz), which is much broader than that of (Ni,Co)@(Ni,Co)$_x$Fe$_{3-x}$O$_4$ chain structures. Thus a much improved microwave absorption performance can be achieved when the ferrite, graphene and magnetic metal particles were assembled into a composite system.

To further understand the microwave absorption properties of the samples, the coefficient of electromagnetic matching (δ) is illustrated by the following equation:

$$\delta = \frac{\mu''/\varepsilon''}{\mu'/\varepsilon'} = \frac{\mu''\varepsilon'}{\mu'\varepsilon''} \quad (3)$$

According to the generalized electromagnetic wave matching theory, the absorber performs better when the δ value is closed to 1, which requires: $\mu'' = \varepsilon''$, and $\mu' = \varepsilon'$. However, the μ and ε value are difficult to satisfy the equation in different frequencies in the same medium because the μ and ε are function of frequency. Figure 5c shows the calculated δ value of (Ni,Co)@(Ni,Co)$_x$Fe$_{3-x}$O$_4$ and (Ni,Co)@(Ni,Co)$_x$Fe$_{3-x}$O$_4$/graphene from 2–18 GHz. It can be found clearly that the δ value of the (Ni,Co)@(Ni,Co)$_x$Fe$_{3-x}$O$_4$/graphene are much closer to constant 1, and the bandwidth of δ = 0-2 are 2-11.52 GHz and 13.04-18 GHz. For (Ni,Co)@(Ni,Co)$_x$Fe$_{3-x}$O$_4$, the bandwidth of δ = 0-2 are 7.68-10.32 GHz and 13.12-18 GHz. These results suggest that the introduction of graphene could improve the equality of the electromagnetic parameters to satisfy the impedance matching condition. To further explore the difference between (Ni,Co)@(Ni,Co)$_x$Fe$_{3-x}$O$_4$ and (Ni,Co)@(Ni,Co)$_x$Fe$_{3-x}$O$_4$/graphene, other important factors that contribute to microwave absorption were also investigated. The eddy currents could generate resistive losses that transform some forms of energy into heat and result in magnetic loss. Theoretically, for a thin sheet with a thickness d, the loss due to the eddy current effect can be evaluated by: $C_0 = \frac{\mu_r''}{\mu_r'^2 f} = \frac{2}{3}\frac{\pi\mu_0 d^2}{\rho}$, where ρ is the electrical resistivity, and μ_0 is the vacuum permeability.[37,38] As shown in Figure 5d, C_0 value of (Ni,Co)@(Ni,Co)$_x$Fe$_{3-x}$O$_4$/graphene composites is higher than (Ni,Co)@(Ni,Co)$_x$Fe$_{3-x}$O$_4$ from 8-18 GHz, indicating that (Ni,Co)@(Ni,Co)$_x$Fe$_{3-x}$O$_4$/graphene provide more magnetic loss. Furthermore, the attenuation constant[39-41] α of (Ni,Co)@(Ni,Co)$_x$Fe$_{3-x}$O$_4$/graphene is also higher than that of (Ni,Co)@(Ni,Co)$_x$Fe$_{3-x}$O$_4$ in frequency range from 7.68-18 GHz (Figure S9†), which signified that the (Ni,Co)@(Ni,Co)$_x$Fe$_{3-}$

$_xO_4$/graphene composites have enhanced dielectric loss and magnetic loss and result in excellent microwave absorption in high frequency range. These results are consistent with the fact that the (Ni,Co)@(Ni,Co)$_x$Fe$_{3-x}$O$_4$/graphene has stronger absorbing ability (RL<-10 dB) at the frequency range of 9.12-16.08 GHz.

The different microwave absorption properties of these two samples can be explained by considering the above magnetic data, δ value with the discussion on the influence of effective complex permittivity and permeability. In our case, the microwave absorption property of (Ni,Co)@(Ni,Co)$_x$Fe$_{3-x}$O$_4$ may be ascribed to their magnetic loss rather than the dielectric loss. The metal@metal oxides hybrid structures retain high magnetism and impedance matching. Its unique structure enhances the dipole interaction when the electromagnetic wave incident into (Ni,Co)@(Ni,Co)$_x$Fe$_{3-x}$O$_4$. When graphene was incorporated into the heterostructure, the absorption performance was affected mainly by the enhanced dielectric loss and electromagnetic matching in the high frequency range because of its enhanced conductivity and eddy current. The presence of the interfacial polarization between graphene and (Ni,Co)@(Ni,Co)$_x$Fe$_{3-x}$O$_4$ can also provide help for enhancing microwave absorption performance.

Conclusion

In summary, a facile strategy based on solvothermal synthesis and partial oxidation process was developed to synthesize (Ni,Co)@(Ni,Co)$_x$Fe$_{3-x}$O$_4$, Ni@Ni$_x$Fe$_{3-x}$O$_4$, Co@Co$_x$Fe$_{3-x}$O$_4$, and (Ni,Co)@Ni$_x$Co$_{3-x}$O$_4$ hybrid structures. As a microwave absorber, (Ni,Co)@(Ni,Co)$_x$Fe$_{3-x}$O$_4$ exhibits the best absorption performance among these materials. (Ni,Co)@(Ni,Co)$_x$Fe$_{3-x}$O$_4$ may display not only a combination of the distinct component properties but also a synergy between different components. The designed core shell structures can keep the inner magnetic metal core from being oxidized and the shell layer with suitable permittivity and permeability is satisfied with the impedance matching. The unique structure enables strong dipole interaction when interacted with the incident microwave field. Furthermore, when the (Ni,Co)@(Ni,Co)$_x$Fe$_{3-x}$O$_4$ was composited with graphene, the presence of the interfacial polarization between graphene and (Ni,Co)@(Ni,Co)$_x$Fe$_{3-x}$O$_4$ can provide help for enhancing microwave absorption performance. The effective absorption (RL<-10 dB) frequency range is about 7.0 GHz (from 9.12 GHz to 16.08 GHz) with the sample thickness of 2.0 mm, which is significantly wider than other reported results. Therefore microwave absorption materials with stronger absorption properties as well as lightweight and broad absorption frequency range can be rationally designed by constructing similar hybrid structures and composites.

Acknowledgements

This work was supported by the National Basic Research Program of China (Grants 2011CBA00508 and 2013CB933901) and the National Natural Science Foundation of China (Grants 21171141, 21333008).

Notes and references

Department of Chemistry & State Key Laboratory of Physical Chemistry of Solid Surfaces, College of Chemistry and Chemical Engineering, Xiamen University, Xiamen, 361005 (China)

E-mail: zyjiang@xmu.edu.cn

†Electronic Supplementary Information (ESI) available: detailed experimental procedures; XPS analysis of (Ni,Co)@(Ni,Co)$_x$Fe$_{3-x}$O$_4$ chains; detailed characterization and microwave absorption properties of Ni@Ni$_x$Fe$_{3-x}$O$_4$, Co@Co$_x$Fe$_{3-x}$O$_4$, (Ni,Co)@Ni$_x$Co$_{3-x}$O$_4$ and graphene. See DOI:10.1039/b000000x/

1 F. J. Ren, H. J. Yu, L. Wang, M. Saleem, Z. F. Tian and P. F. Ren, *RSC Adv.,* 2014, **4**, 14419.
2 L. B. Kong, Z. W. Li, L. Liu, R. Huang, M. Abshinova, Z. H. Yang, C. B. Tang, P. K. Tan, C. R. Deng and S. Matitsine, *Int. Mater. Rev.,* 2013, **58**, 203.
3 F. Qin and C. Brosseau, *J. Appl. Phys.,* 2012, **111**, 061301.
4 S. Chandrasekaran, S. Ramanathan and T. Basak, *AIChE Journal,* 2012, **58**, 330.
5 Z. F. Zi, J. M. Dai, Q. C. Liu, H. Y. Liu, X. B. Zhu and Y. P. Sun, *J. Appl. Phys.,* 2011, **109**, 07E536.
6 F. L. Wang, J. R. Liu, J. Kong, Z. J. Zhang, X. Z. Wang, M. Itoh and K. i. Machida, *J. Mater. Chem.,* 2011, **21**, 4314.
7 J. Wei, J. H. Liu and S. M. Li, *J. Magn. Magn. Mater.,* 2007, **312**, 414.
8 S. J. Yan, L. Zhen, C. Y. Xu, J. T. Jiang, W. Z. Shao and J. K. Tang, *J. Magn. Magn. Mater.,* 2011, **323**, 515.
9 M. G. Han, D. F. Liang and L. J. Deng, *Appl. Phys. Lett.,* 2011, **99**, 082503.
10 Y. X. Gong, L. Zhen, J. T. Jiang, C. Y. Xu and W. Z. Shao, *J. Appl. Phys.,* 2009, **106**, 064302.
11 J. R. Liu, M. Itoh, M. Terada, T. Horikawa and K. i. Machida, *Appl. Phys. Lett.,* 2007, **91**, 093101.
12 K. P. Yuan, R. C. Che, Q. Cao, Z. K. Sun, Q. Yue and Y. H. Deng, *ACS Appl. Mater. Interfaces,* 2015, **7**, 5312.
13 S. J. Yan, L Zhen, C. Y. Xu, J. T. Jiang and W. Z. Shao, *J. Phys. D: Appl. Phys.,* 2010, **43**, 245003.
14 X. J. Zhang, G. S. Wang, W. Q. Cao, Y. Z. Wei, J. F. Liang, L. Guo and M. S. Cao, *ACS Appl. Mater. Interfaces,* 2014, **6**, 7471.
15 H. Zhang, A. J. Xie, C. P. Wang, H. S. Wang, Y. H. Shen and X. Y. Tian, *J. Mater. Chem. A,* 2013, **1**, 8547.
16 L. Zhang and H. Zhu, *Mater. Lett.,* 2009, **63**, 272.
17 G. Z. Wang, Z. Gao, S. W. Tang, C. Q. Chen, F. F. Duan, S. C. Zhao, S. W. Lin, Y. H. Feng, L. Zhou and Y. Qin, *ACS Nano,* 2012, **6**, 11009.
18 Z. Y. Chu, H. F. Cheng, W. Xie and L. K. Sun, *Ceram. Int.,* 2012, **38**, 4867.
19 N. J. Tang, W. Zhong, C. T. Au, Y. Yang, M. G. Han, K. J. Lin and Y. W. Du, *J. Phys. Chem. C,* 2008, **112**, 19316.
20 X. C. Zhao, Z. M. Zhang, L. Y. Wang, K. Xi, Q. Q. Cao, D. H. Wang, Y. Yang and Y.W. Du, *Sci. rep.,* 2013, **3**, 3421.
21 Y. L. Ren, H. Y. Wu, M. M. Lu, Y. J. Chen, C. L. Zhu, P. Gao, M. S. Cao, C. Y. Li and Q. Y. Ouyang, *ACS Appl. Mater. Interfaces,* 2012, **4**, 6436.
22 M. Zong, Y. Huang, Y. Zhao, X. Sun, C. H. Qu, D. D. Luo and J. B. Zheng, *RSC Adv.,* 2013, **3**, 23638.

23 A. M. Nicolson and G. F. Ross, *IEEE Trans. Instrum. Meas.,* 1970**,** **19** , 377.
24 Y. S. Yu, A. Mendoza-Garcia, B. Ning and S. H. Sun, *Adv. Mater.,* 2013, **25**, 3090.
25 R. C. Che, C. Y. Zhi, C. Y. Liang and X. G. Zhou, *Appl. Phys. Lett.,* 2006, **88**, 033105.
26 S. Mallégol, C. Brosseau, P. Quéffelec and A.M. Konn, *Phys. Rev. B,* 2003**,** **68**, 174422.
27 K. V. Rao and A. Smakula, *J. Appl. Phys.,* 1965, **36**, 2031.
28 L. Wang, Y. Huang, X. Sun, H. J. Huang, P. B. Liu, M. Zong and Y. Wang, *Nanoscale,* 2014, **6**, 3157.
29 L. Z. Wu, J. Ding, H. B. Jiang, L. F. Chen and C. K. Ong, *J. Magn. Magn. Mater.,* 2005, **285**, 233.
30 L. Z. Wu, J. Ding, H. B. Jiang, C. P. Neo, L. F. Chen and C. K. Ong, *J. Appl. Phys.,* 2006, **99**, 083905.
31 C. Brosseau and P. Talbot, *J. Appl. Phys.,* 2005, **97**, 104325.
32 Y. P. Duan, Y. H. Zhang, T. M. Wang, S. C. Gu, X. Lin and X. J. Lv, *Mater. Sci. Eng. B,* 2014, **185**, 86.
33 Q. H. Liu, X. H. Xu, W. X. Xia, R. C. Che, C. Chen, Q. Cao and J. G. He, *Nanoscale*, 2015, **7**, 1736.
34 X. T. Zhan, H. Z. Tang, Y. Du, A. Talbi, J. L. Zha and J. H. He, *RSC Adv.*, 2013, **3**, 15966.
35 B. Zhao, G. Shao, B. B. Fan, W. Y. Zhao, Y. J. Xie and R. Zhang, *RSC Adv.*, 2014, **4** ,61219.
36 F. X. Qin, J. Tang, V. V. Popov, J. S. Liu, H. X. Peng and C. Brosseau, *Appl. Phys. Lett.,* 2014, **104**, 012901.
37 X. Gu, W. M. Zhu, C. J. Jia, R. Zhao, W. Schmidt and Y. Q. Wang, *Chem. Commun.*, 2011, 47, 5337.
38 X. Sun, J. P. He, G. X. Li, J. Tang, T. Wang, Y. X. Guo and H. R. Xue, *J. Mater. Chem. C*, 2013, **1**, 765.
39 B. Lu, H. Huang, X. L. Dong, X. F. Zhang, J. P. Lei, J. P. Sun and C. Dong, *J. Appl. Phys.* , 2008, **104**, 114313.
40 S. L. Wen, Y. Liu, X. C. Zhao, J. W. Cheng and H. Li, *Phys. Chem. Chem. Phys.*, 2014, **16**, 18333.
41 B. Zhao, G. Shao, B. B. Fan, W. Y. Zhao and R. Zhang, *Phys. Chem. Chem. Phys.*, 2015, **17**, 2531.

Facile synthesis of (Ni,Co)@(Ni,Co)$_x$Fe$_{3-x}$O$_4$ core@shell chain structures and (Ni,Co)@(Ni,Co)$_x$Fe$_{3-x}$O$_4$/graphene composites with enhanced microwave absorption

Yuan Lin, Lu Xu, Zhiyuan Jiang,* Hongli Li, Zhaoxiong Xie and Lansun Zheng

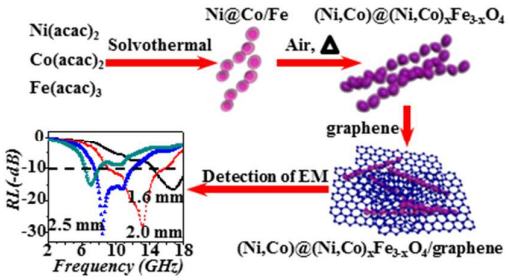

A facile strategy was developed to fabricate (Ni,Co)@(Ni,Co)$_x$Fe$_{3-x}$O$_4$ chain structures and (Ni,Co)@(Ni,Co)$_x$Fe$_{3-x}$O$_4$/graphene composites, which show excellent microwave absorption performances.